Applied Geography 97 (2018) 35–47

Contents lists available at ScienceDirect

Applied Geography

journal homepage: www.elsevier.com/locate/apgeog

Examining impacts of the Belo Monte hydroelectric dam construction on land-cover changes using multitemporal Landsat imagery

Xiandie Jiang[a], Dengsheng Lu[a,b,c,d,*], Emilio Moran[d], Miquéias Freitas Calvi[e], Luciano Vieira Dutra[f], Guiying Li[b,c]

[a] State Key Laboratory of Subtropical Silviculture, School of Environmental & Resource Sciences, Zhejiang Agriculture and Forestry University, Hangzhou 311300, China
[b] Fujian Provincial Key Laboratory for Subtropical Resources and Environment, Fujian Normal University, Fuzhou 350007, China
[c] School of Geographical Sciences, Fujian Normal University, Fuzhou 350007, China
[d] Center for Global Change and Earth Observations, Michigan State University, East Lansing, MI 48823, USA
[e] Faculty of Forestry, Federal University of Pará, Altamira, PA 68372-040, Brazil
[f] National Institute for Space Research, Av. dos Astronautas, 1758, São Jose dos Campos, SP 12245-010, Brazil

ARTICLE INFO

Keywords:
Belo Monte hydroelectric dam
Land-cover change
Impacts of dam construction
Post-classification comparison
Multitemporal Landsat imagery

ABSTRACT

Many hydroelectric dams in the Brazilian Amazon have been constructed, but how dam construction influences land-cover change has not been fully examined. For our research, we selected Belo Monte hydroelectric dam, the third-largest dam in the world, to explore its impacts on major land-cover change. Multitemporal Landsat images between 2006 and 2017 were used. The maximum likelihood classifier was used to classify these Landsat images into primary forest, secondary forest, agropasture, man-made bare land, natural bare land, and water. The land-cover change was examined using the post-classification comparison approach based on different stages of dam construction, and was further examined along the upstream and downstream river buffer. The results indicate that overall classification accuracies of 89.7% and 92.3% were obtained for the 2011 and 2015 land-cover classification results, respectively. Primary forest decreased continuously from 47.8% in 2006 to 35.3% in 2017. Different stages of dam construction had various impacts, that is, before dam construction, deforestation and agropasture expansion were the major land-cover change categories; during dam construction, the increased area of man-made bare lands, the canal construction zone, and the increased area of natural bare lands downstream were obvious, in addition to deforestation and agropasture dynamics; when dam construction was complete, water bodies increased considerably upstream and decreased downstream. These big changes in water bodies may have long-term impacts on ecosystem functions and environments. This research provides new insights on the impacts of dam construction on land-cover changes, which is valuable for making better decisions about water and land resources.

1. Introduction

Since the 1970s, economic development, industrialization, and demographic growth have resulted in increasing demand for energy. This developmental pathway has led to strategies that give priority to the expansion of electric energy production (Bermann, 2001; Moretto, Gomes, Roquetti, & Jordão, 2012). As happened earlier in the USA and Europe, the strategy in Brazil gave importance to the construction of hydroelectric dams (Moran, 2016), and with priority given to the region with the highest hydroelectric potential: The Amazon. The region has a high potential for production of energy estimated at 77 GW (Brasil, 2007) and is considered the frontier for hydropower development with 352 dams planned, of which 96 will be hydroelectric and 256 will be smaller ones capable of generating energy (Aneel, 2017). The Belo Monte dam on Xingu River is the largest one in the Amazon.

Studies conducted in the 1970s projected the construction of up to six large dams that would have created flooded areas covering 17,610 km^2 (Sevá, 2005). The negative impacts associated with these projects, especially the flooding of territories of 37 indigenous groups, led to social mobilization opposing the construction of dams, with national and international attention brought to bear (Fearnside, 2015, 2017). These considerations, as well as difficulties in financing such dams in the 1990s (Moretto et al., 2012), kept the project from going forward. In the first decade of the 21st century, the project came back to

* Corresponding author. State Key Laboratory of Subtropical Silviculture, School of Environmental & Resource Sciences, Zhejiang Agriculture and Forestry University, Hangzhou 311300, China.
E-mail addresses: xiandiej@163.com (X. Jiang), dengshenglu@gmail.com (D. Lu), moranef@msu.edu (E. Moran), mcalvi@ufpa.br (M.F. Calvi), dutra@dpi.inpe.br (L.V. Dutra).

https://doi.org/10.1016/j.apgeog.2018.05.019
Received 28 February 2018; Received in revised form 22 May 2018; Accepted 27 May 2018
Available online 01 June 2018
0143-6228/

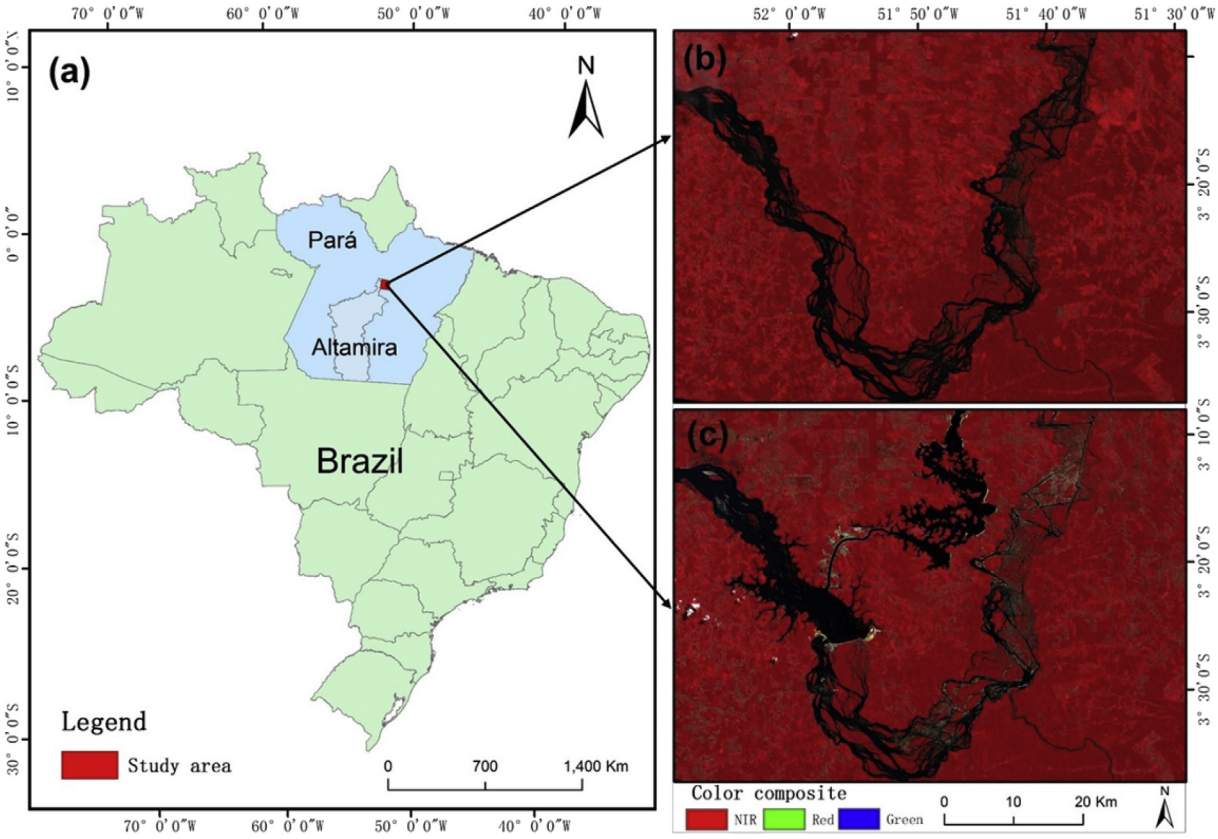

Fig. 1. Location of the study area (a) and color composites in 2011 (b) and 2016 (c) with Landsat spectral bands NIR, red, and green mapped in RGB. (For interpretation of the references to color in this figure legend, the reader is referred to the Web version of this article.)

life as a response to concerns with deficits in energy production due to lower precipitation and lower energy production in existing dams—and a lack of planning and investment in the energy sector (Fearnside, 2003; Hage, 2012). Up to 2002, the energy matrix of Brazil depended on hydropower for 80% of energy production (Aneel, 2002), a situation of high risk due to a lack of diversified energy sources.

To speed up construction of Belo Monte, the Brazilian government and the construction companies redesigned the project to reduce the size of the area to be flooded to avoid flooding indigenous areas. This redesign increased the power production and made the project the third largest in the world in terms of energy production, i.e., 11 GW. The magnitude of the project—the largest infrastructure project undertaken by the government during the first decade of the 21st century—provoked the largest resettlement of people and greatest negative environmental impacts (Maia, Guerra, & Calvi, 2017). It led to rapid population increase (Moran, 2016), expansion of the urban area, and changes in the landscape (Feng et al., 2017).

The impacts of dam construction on population displacement, fisheries, biodiversity loss, and ecosystem functions and services have long been recognized (Fearnside, 2014, 2016, 2017). Chen, Powers, de Carvalho, and Mora (2015) examined the impacts of the Tucuruí Dam in the State of Pará, Brazil, on deforestation and degradation, but the impacts may be much more extensive and intensive in Belo Monte, and would include other land covers too. Studying the effects of Belo Monte dam on the surrounding environment is highly relevant given the scale and importance of the project for the local area, and because it is just one of many hydropower dams planned for the Amazon region. Understanding the land-cover transformations is also relevant to discussions of climate change, and to debates over the impacts that dams have on land-cover change. There has been a notable lack of assessments of the areas transformed by the building of dams and filling of reservoirs. In the past, construction companies have routinely underestimated the areas flooded by dams and the land-cover changes resulting therefrom. It is important to understand how different stages of dam construction—before, during, and after influence land-cover change.

The unique characteristic of remotely sensed data in data collection and representation of land surfaces has made it the primary data source for land-use/cover classification and change detection in the past four decades. A large number of studies have been conducted to explore the approaches to improve land-cover classification (see the review paper by Lu & Weng, 2007) and change detection accuracies (see the review papers by Lu, Mausel, Brondízio, & Moran, 2004, 2014). Although many classifiers such as maximum likelihood classifier (MLC), minimum distance, decision tree, and artificial neural network are available (M. Li, Zang, Zhang, Li, & Wu, 2014; Lu & Weng, 2007; Salah, 2017), MLC is often used for land-cover classification because it can provide similar or even more accurate classification results, especially when only spectral bands are used (G. Li, Lu, Moran, & Hetrick, 2011, 2012; Lu, Li, Moran, Dutra, & Batistella, 2011, 2012). Considering remote sensing–based change detection techniques, most of the algorithms such as principal component analysis, image differencing, and regression can only detect binary change and non-change information (Coppin, Jonckheere, Nackaerts, Muys, & Lambin, 2004; Erasu, 2017; Lu et al., 2004; Singh, 1989). However, in reality, we need to know the detailed “from-to” land-cover change trajectories (Lu, Li, & Moran, 2014). The post-classification comparison is commonly used for detecting land-cover trajectories (Han, Zhang, & Zhou, 2018; Lu, Li, Moran, & Hetrick, 2013; Tewkesbury, Comber, Tate, Lamb, & Fisher, 2015; Zhu, 2017). The key is to develop accurate land-cover classification result for each date.

Considering the stages of dam construction in this research, remote sensing data availability, and the characteristics of landscape under investigation, multitemporal Landsat images from 2006 to 2017 were selected to examine land-cover distribution and dynamic changes. The

objective of this research was to examine the impacts of different dam construction stages on land-cover changes, especially deforestation, urbanization, dynamic change between secondary forest and agropoasture, and water area change in this region. Through this analysis, we can better understand the relationships between dam construction and land-cover change, providing fundamental data sources for making better decisions in land resource management.

2. Study area

The study region is located among the northeastern municipalities of Altamira in Pará State in the eastern Amazon (Fig. 1). The area was first occupied by indigenous people who were resettled with the arrival of the construction crews of the TransAmazon Highway in 1971. The urban area of Altamira had been a trading center for wild rubber that saw its economic peak between 1870 and 1912, and a smaller boom during World War II when supplies from Malaysia were cut off by the Japanese and the Allies turned to Brazil to increase production needed for the war effort (Moran, 1975, 1981). Between 1971 and 2010, the Altamira region was a prosperous agropastoral region, blessed with good soils and hardworking people who came to settle along the highway (Moran, 2016). Studies in the area over the years have tracked the occupation of the area, its land-use changes, and the gradual dominance of cattle and cocoa in many of the farms. The major land covers include primary forest, secondary forest, cocoa plantations, agricultural lands, pastures, bare soils, impervious surfaces, and water. The study area is in moist tropical region with annual precipitation as high as 2700 mm in 2006 and as low as 1600 mm in 2015 based on local weather station data. The dry season begins in June and lasts until October.

Discussion of a dam in the region goes as far back as the 1970s when geologists identified what they thought were ideal conditions for hydropower generation. However, the plans proposed met strong opposition from indigenous groups and from civil society concerned with the negative social and environmental impacts of a large dam. Only in 2010, by presidential fiat, was the authorization to begin construction given (Moran, 2016). The construction began in 2011 and finished in 2016 (though installation of all 24 turbines will not be complete until 2019). Thus, for the purposes of this analysis, we have divided the changes into three major stages: preparation stage before 2011, construction stage between 2011 and 2015, and finished stage after 2016 when the reservoirs were filled. The land-cover changes were considerably different in each time period, and it is necessary to examine the different change trajectories to understand the impacts of dam construction on land-use/cover change in this region.

3. Materials and methods

3.1. Collection and preprocessing of remote sensing data

In the Brazilian Amazon, cloud cover is often a problem resulting in difficulty of collecting good-quality optical sensor data (Asner, 2001), and cloud-free Landsat images for certain years were not available for our research, as shown in Table 1. For example, there are no useful images for the years of 2012–2014. There are some clouds and shadows in the Landsat Thematic Mapper (TM) images in 2006, 2008, 2011, and Landsat Operational Land Imager (OLI) in 2016, and we had to replace them with other Landsat images. The images were atmospherically calibrated with the dark-object subtraction approach (Chander, Markham, & Helder, 2009; Chavez, 1996). The images with clouds/shadows were then normalized with another image using the relative calibration approach based on unchanged objects in both images (Vicente-Serrano, Perez-Cabello, & Lasanta, 2008) to replace clouds and shadows. Fmask was used to detect clouds and shadows in the Landsat images (Qiu, He, Zhu, Liao, & Quan, 2017). Topographic correction was not conducted for these images due to the lack of good-quality digital elevation model data and because the terrain did not seriously affect the surface reflectance in this region.

The Satellite Pour l'Observation de la Terre (SPOT) imagery, acquired on August 19, 2015, was used to collect sample plots of different land covers based on visual interpretation. The SPOT image has four multispectral bands (e.g., three visible bands and one near-infrared band) with 6 m spatial resolution and one panchromatic band with 1.5 m spatial resolution. In order to improve visual interpretation effectiveness, improvement of spatial resolution through data fusion is helpful (Lu et al., 2011; Pohl & van Genderen, 1998; Zhang, 2010). Based on comparison of common data fusion approaches, such as principal component analysis, intensity-hue-saturation, and Gram-Schmidt Pan Sharpening (GS), the GS fusion approach was used for the fusion of the SPOT multispectral and panchromatic data because this approach can keep the fidelity of spectral features while improving spatial resolution, a conclusion similar to previous research (e.g., Karathanassi, Kolokousis, & Ioannidou, 2007; Laben & Brower, 2000). In addition to the high spatial resolution images, a large number of sample plots with different land covers (e.g., primary forest, secondary forest, cocoa plantations, pasture, impervious surfaces, bare soils, agricultural lands) were collected during fieldwork with GPS in August 2015.

3.2. Land-cover classification and accuracy assessment

Based on our field survey and research objectives, we designed a classification system of six land covers: primary forest (PF), secondary forest (SF), agropasture (AP), man-made bare land (ML), natural bare land (NL), and water (WA). Here ML represents the impervious surfaces (e.g., buildings, roads) and bare soils produced in the dam and canal construction areas by human activities. NL is referred to as bare lands (e.g., mud, sand, rocks) along the rivers due to WA decrease. In this study area, cocoa plantations were rapidly expanded. Our field survey indicated that they have various densities and are often mixed with other tree species. Their stand structure is more like SF than pasture, and cocoa plantations cannot be successfully separated from SF in Landsat images, thus they were grouped into the SF category.

Before reducing the number of land covers for our research, the initial land-cover types included impervious surfaces, bare lands near the buildings and in the construction zones, bare lands along the rivers, WA, PF, initial/intermediate/advanced succession (different stages of SF), pasture, and croplands. Clouds and shadows were also selected as special types during the classification procedure. Based on field survey and visual interpretation of the 2015 SPOT fused image with 1.5 m spatial resolution, a total of 360 sample plots with a minimum number of 30 plots for each land-cover type were collected in 2015. These training samples were selected from the 2015 Landsat OLI data with window sizes of 3 by 3 or 5 by 5, depending on the patch sizes of different land covers. The separability analysis with transformed divergence was conducted to optimize the training samples for each land cover (Mausel, Kramber, & Lee, 1990). The training samples for each land cover were overlaid on the 2016 and 2017 Landsat color composites separately to modify the land covers based on visual interpretation. Meanwhile, a total of 350 sample plots from 2011 were selected from the RapidEye image and overlaid on the 2006 and 2008 Landsat color composites for modification.

MLC was used to classify Landsat multispectral imagery based on training samples. The classified image was further modified using majority filtering with a window size of 3 by 3 pixels to remove the salt-and-pepper problem (Erasu, 2017; Lu & Weng, 2007). In the classified images, a very limited number of clouds and shadows still existed, and they were modified based on visual interpretation on the color composites. For all the classified images, some expert rules were further used to improve the classification results. For example, if the pixels were classified as SF in one image but PF on the posterior date, the pixels in the posterior image were modified to SF. In this way, the

Table 1
Datasets used in research.

Dataset	Image acquisition dates	Description
Landsat 8 OLI (path/row: 225/62)	July 20, 2017 August 2, 2016 (July 17, 2016) July 15, 2015	Six Landsat multispectral bands (visible, near-infrared, and short-wavelength infrared) with spatial resolution of 30 m were used for land-cover classification.
Landsat 5 TM	July 4, 2011 (July 27, 2011) July 11, 2008 (June 23, 2007) June 20, 2006 (June 4, 2006)	
SPOT 6	August 19, 2015	Four multispectral bands with spatial resolution of 6 m and one panchromatic band with1.5 m. The Gram-Schmidt Pan Sharpening approach was used to integrate both multispectral and panchromatic data into a new data, and the fused image was used to collect sample plots for different land covers through visual interpretation.
RapidEye	July 28, 2011	Ground sampling distance (nadir): 6.5 m; pixel size: 5 m. The RapidEye image was used to collect validation samples for evaluation of land-cover classification in 2011.
Fieldwork	August 2015	Many samples for different land-cover types were collected and randomly selected for use as training samples and test samples.
Weather data	January 2006–August 2017	Temperature, precipitation, evaporation, etc. were collected

Note: TM, Thematic Mapper; OLI, Operational Land Imager; SPOT, Satellite Pour l'Observation de la Terre.

Table 2
A summary of different stages of Belo Monte dam construction.

Time	Stages	Description of key events at each stage
2006–2008	Before dam construction	Studies begin on environmental impact; Farmers continue to expand pastures and cultivated areas
2008–2011	Preparation for dam construction	Completion of environmental impact studies; License to start building the dam issued; Start of construction and roads paved to improve infrastructure capacity; Families notified of impending resettlement; Farmers start reducing their activities near the reservoir-to-be
2011–2015	Middle stage of dam construction	Hundreds of families resettled compulsorily; Removal of vegetation from future reservoir area; Authorization to fill the reservoir and issuing license to operate
2015–2016	Near-completion stage	Advanced stage of construction; Areas no longer needed for construction begin to be ceded to farmers to reoccupy; Start of energy production
2016–2017	After-completion stage	Drought brings about difficulties in navigation

confusion between PF and advanced SF was reduced. ML and NL were difficult to separate based on their spectral signatures, but their distribution had specific characteristics to help in separation; for example, ML was located mainly in the dam and canal construction areas, and NL was located along the river due to the decreased WA. ML was also confused with some agricultural lands after harvest because of their similar spectral features, but knowing their different spatial distributions enabled us to separate them.

Accuracy assessment was conducted using the error matrix–based approach (Congalton & Green, 2008; Foody, 2002). A stratified random sampling approach was used, and a total of 300 sample plots with a minimum of 30 sample plots for each land-cover type were selected. The field survey data and fused SPOT image of 2015 were used to support the identification of reference data for evaluation of the 2015 Landsat image classification results. Meanwhile, the RapidEye images from 2011 were also used to collect sample plots for validation of the 2011 land-cover classification result. Because no field survey data and/or high spatial resolution images were available for other years for land-cover classification, no accuracy assessment was conducted. From the error matrix, overall classification accuracy and kappa coefficient were used to assess the overall classification results; producer's and user's accuracies were used to evaluate each land-cover classification result (Congalton & Green, 2008).

3.3. Analysis of land-cover change detection and impacts of dam construction

The land-cover change analysis was conducted using the post-classification comparison approach at the different stages between 2006 and 2017. Based on data availability and the time period of dam construction, the change detection periods are separated into five stages, as summarized in Table 2. The dam construction may considerably influence the nearby land-cover change, especially WA, ML, NL, and AP. Therefore, in addition to the analysis of land-cover change trajectories over the entire study area, more emphasis is on the land-cover change along the river. Considering the spatial resolution of Landsat imagery (i.e., 30 m), the spatial patterns of river distribution, and extent of the study area, a buffer zone of 2 km along both sides of the river was produced based on the classified water data (e.g., river here) in 2006 (see Fig. 2). The 2 km buffer seems optimal, because a too-small buffer would not have included a sufficient number of pixels away from the river, while a too-large buffer would have extended beyond the boundary of the study area. Meanwhile, the newly established dam was selected to separate the river into upstream and downstream to further examine the different impacts of this dam construction on land-cover changes.

4. Results

4.1. Analysis of land-cover classification results

The overall classification accuracies for 2011 and 2015 (Table 3) were 89.7% and 92.3%, respectively. The major errors were from the confusions between advanced succession SF and PF due to their similar forest stand structures, between initial succession SF and AP (e.g., dirty pasture), and between AP and ML (similar features between croplands

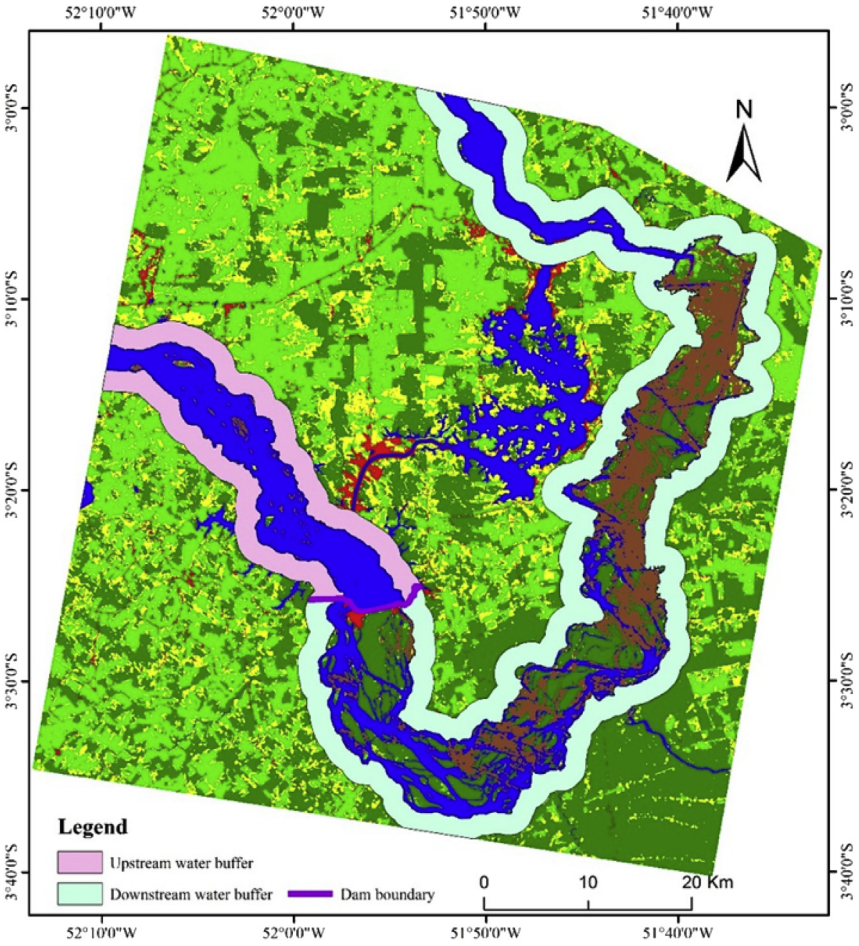

Fig. 2. Analysis of 2-km-wide buffer zones along the river upstream and downstream from the Belo Monte dam in Brazil using the base of a 2006 image.

Table 3
Accuracy assessment of land-cover classification results in 2011and 2015.

Year	Type	Reference data										Overall accuracy
		PF	SF	AP	ML	NL	WA	CT	RT	UA	PA	
2011	PF	103	1	0	1	1	0	106	108	97.2	95.4	OA = 89.7%
	SF	4	23	2	0	0	0	29	31	79.3	74.2	KC = 0.87
	AP	0	7	64	6	1	0	78	70	82.1	91.4	
	ML	0	0	4	23	0	0	27	30	85.2	76.7	
	NL	0	0	0	0	27	2	29	30	93.1	90.0	
	WA	1	0	0	0	1	29	31	31	93.5	93.5	
2015	PF	104	2	1	0	0	1	108	106	96.3	98.1	OA = 92.3%
	SF	2	27	3	0	0	0	32	33	84.4	81.8	KC = 0.90
	AP	0	4	63	4	2	0	73	71	87.7	90.1	
	ML	0	0	4	26	0	0	30	30	90.0	90.0	
	NL	0	0	0	0	28	0	28	30	100.0	93.3	
	WA	0	0	0	0	0	29	29	30	100.0	96.7	

Note: PF, primary forest; SF, secondary forest; AP, agropoasture; ML, man-made bare land; NL, natural bare land; WA, water; CT, column total; RT, row total; UA, user's accuracy; PA, producer's accuracy; OA, overall classification accuracy; KC, kappa coefficient.

in dry season and bare soils). The land-cover classification results from 2006 to 2017 (Fig. 3) clearly show the increased WA area along the canal in 2016 and 2017 and decreased WA area downstream. Another obvious change was the increased ML in 2015 due to the canal construction, then most ML area was replaced with WA in 2016 due to the completion and operation of the dam.

Overall, PF decreased considerably from 47.8% in 2006 (2178 km^2) to 35.3% in 2017 (1608 km^2), SF remained stable, except decreasing between 2008 and 2011 by about 2% (Table 4). AP area increased before the dam construction (2006–2011), and remained stable during and after dam construction. The proportion of ML was small before the dam construction, but sharply increased in 2015, as shown in Fig. 3, due to the canal construction, then decreased in 2016 due to the increased WA. NL had a small proportion in 2006, but sharply increased in 2008, and continuously increased from 2015 to 2017; as shown in Fig. 3, the decreased WA downstream resulted in the NL increase along the river.

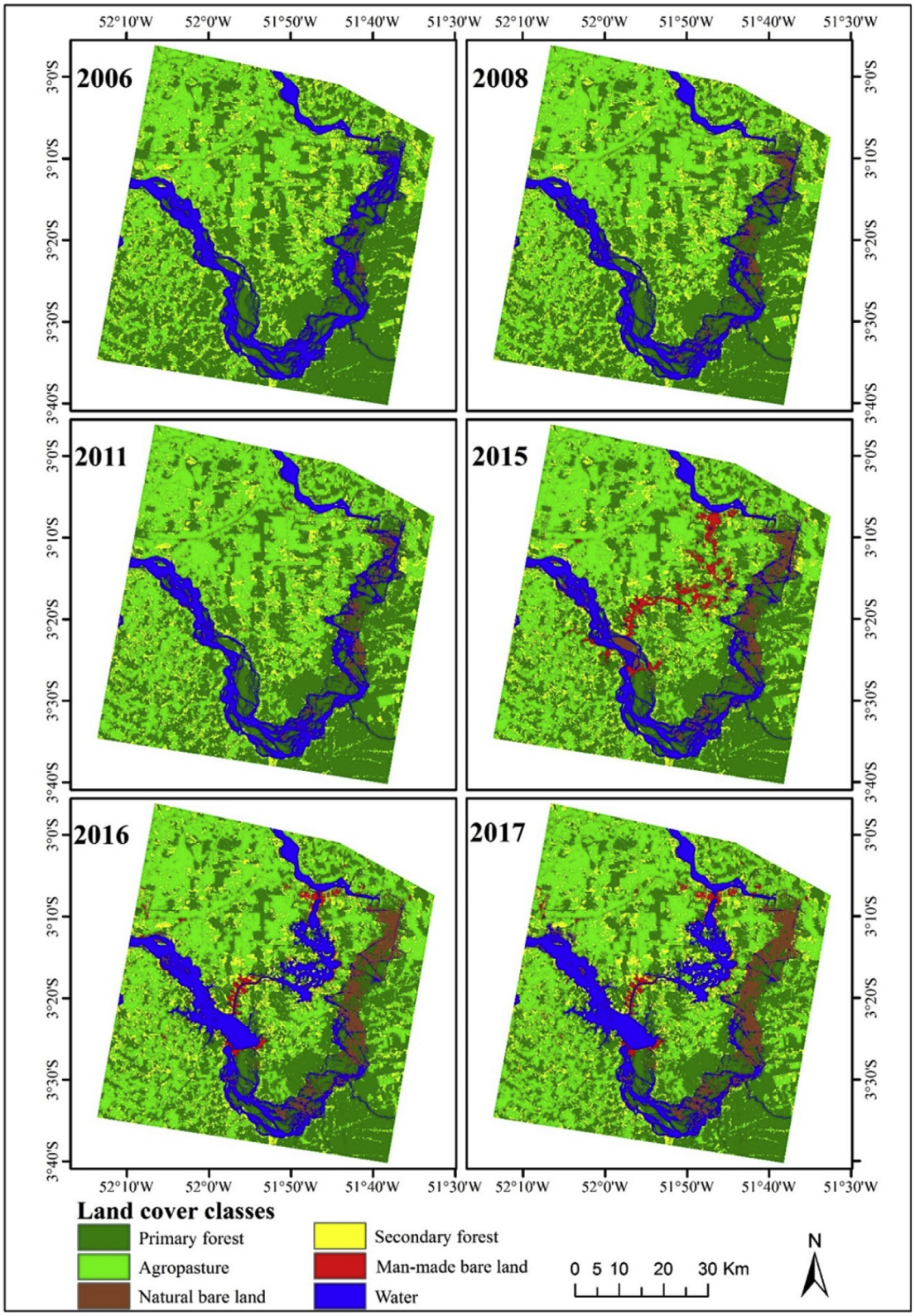

Fig. 3. Spatial distribution of land covers at specific points in time in the area surrounding the Brazilian Belo Monte dam (constructed 2011–2015).

4.2. Analysis of land-cover change detection results

Table 5 indicates that during the whole detection period between 2006 and 2017, PF and SF decreased, but AP, ML, NL, and WA increased, and the major changes were PF deforestation and AP and NL expansions. However, the average annual change rates varied considerably in different detection periods. For example, between 2006 and 2008, PF deforested area almost equaled AP expansion area, and the increased NL area almost equaled the decreased WA area. Between 2008 and 2011, the PF and SF losses were due to AP expansion; however, between 2011 and 2015, the PF loss was due to ML increase, and the WA loss resulted in the NL increase, as shown in Fig. 4. A big

Table 4
Area and percentage of each land cover at specific years.

Land cover	Area (km^2) of each land cover at specific years					
	2006	2008	2011	2015	2016	2017
Primary forest	2177.88	2014.22	1899.76	1743.73	1655.35	1608.49
Secondary forest	729.56	732.72	637.15	634.34	641.78	633.82
Agropasture	1078.36	1241.51	1425.82	1422.88	1381.91	1384.40
Man-made bare land	23.27	23.89	28.27	158.91	102.41	115.01
Natural bare land	38.70	123.04	105.37	183.76	229.14	252.05
Water	507.82	420.20	459.22	411.98	545.01	561.83
	Percentages of each land cover at specific years					
Primary forest	47.81	44.21	41.70	38.28	36.34	35.31
Secondary forest	16.01	16.08	13.99	13.92	14.09	13.91
Agropasture	23.67	27.25	31.30	31.23	30.33	30.39
Man-made bare land	0.51	0.52	0.62	3.49	2.25	2.52
Natural bare land	0.85	2.70	2.31	4.03	5.03	5.53
Water	11.15	9.22	10.08	9.04	11.96	12.33

Note: Percentage of the *i*th land cover (A_i) to total area (A): $A_i\% = (Ai/A)*100$.

difference in Table 5 shows that between 2015 and 2016, the large decreases in PF, AP, and ML resulted in large increases for WA and NL due to the completed dam construction, whereas between 2016 and 2017, the PF deforestation resulted in the increases in ML, NL, and WA. These changes in different land covers were related to the stages of dam construction. As shown in Fig. 4, the major changes in WA, ML, and NL occurred along the river and the newly constructed canal in the central part of this study area. For example, the large increase in WA in the central part and upstream occurred between 2015 and 2016 due to the completed dam and canal construction (Fig. 4a1); the large increase in ML occurred between 2011 and 2015 in the central part due to the canal construction (Fig. 4b1).

Table 6 adds to the information provided in Table 5 by providing details of the trajectories of the land-cover changes. Large deforestation due to the conversion from PF to SF and AP, large AP expansion at the cost of PF and SF, and a large decrease in WA due to the conversion to NL caused by dry weather occurred between 2006 and 2008 (Table 6). The period between 2008 and 2011 witnessed continuous AP expansion at the cost of SF, and PF conversion to SF and AP. Another obvious change in 2008–2011 was the conversion from NL to WA. Conversely, WA area decreased, and ML and NL increased considerably from 2011 to 2015. The increased ML was mainly from the conversion of PF, SF, and AP, and the increased NL was due to the conversion of WA in this period. A huge dynamic change between 2015 and 2016 was the increased WA from the conversion of AP, ML, and NL upstream, and the conversion of WA to NL downstream. Deforestation due to the conversion from PF to SF and AP and dynamic changes between SF and AP were obvious. The completion of dam construction resulted in considerably different land-cover changes compared to previous detection periods. In 2016 and 2017, the area with land-cover changes was much smaller than in previous years, although deforestation still occurred and upstream WA increased continuously. Fig. 5 clearly shows the spatial patterns of major land-cover change trajectories. The most obvious changes occurred along the river and the newly constructed canal in 2011–2015 and 2015–2016.

4.3. The impacts of dam construction on land-cover change

Dam construction indeed considerably influenced the water distribution—the total water areas changed from 377.6 to 464.3 km^2 between 2006 and 2011 (before dam construction) to 362.5–386.4 km^2 (during and after dam construction) (see Table 7). In particular, the water areas upstream and downstream before and after dam construction changed significantly. For example, the upstream water area was 120.5–129.0 km^2 before the dam was constructed (i.e., before 2015), much smaller than the area of 183.8–199.9 km^2 after the dam was completed and functioning in 2016–2017. Conversely, the downstream water area was 241.3–335.3 km^2 before 2015, much higher than the area of 186.5–193.3 km^2 in 2016–2017. Fig. 6 clearly shows the spatial patterns of water changes upstream and downstream and in the newly constructed canal, which redirects water to the turbines. These results show that dam construction resulted in considerable increase in water area upstream and decrease downstream, in addition to the increased water area along the canal in the central part of this study area.

Table 8 provides further detailed WA change trajectories. In 2006–2008, very limited WA area increased along the river, but the conversion from WA to NL reached 38.3 km^2 downstream. In 2008–2011, an obvious WA change was inundation of the NL area (about 10.2 km^2) downstream. Conversely, the major WA change was the conversion to NL in 2011–2015. After dam construction was finished in 2016, WA increased by 64 km^2 upstream at the cost of mainly AP, ML, and NL, but decreased by 53 km^2 downstream and converted to NL. The year 2016–2017 had a WA change similar to that in 2015–2016, but in a much smaller area. The results in Table 8 document the great impacts of dam construction on WA change in the upstream and downstream regions. The impacts of different stages of dam construction on land-cover change can be summarized as follows:

1) Before stage (before 2011): The major land-cover changes included deforestation (from PF to AP and SF), agricultural expansion (from PF and SF to AP), and the dynamic change between SF and AP. The change between WA and NL was mainly due to the weather conditions.
2) Middle stage (2011–2015): Deforestation was obvious, but almost evenly converted to SF, AP, and ML. SF remained stable, but gained from the conversion of PF to SF and lost due to the conversion from SF to AP. The important changes were the increased area of ML near the dam construction site and the canal construction zone due to conversion from PF, SF, and AP, and the increased area of NL due to conversions from WA and PF.
3) Near completion stage (2015–2016): The land-cover change in this period was considerably different from other periods. The decreased area in PF, AP, and ML resulted in large, increased areas of WA and NL. The finished dam construction greatly influenced the land-cover change; for example, WA area increased considerably upstream and

Table 5
Changed area (km^2) of each land cover at different detection periods.

Type	Overall changed area (km^2) (2006–2017)	Annual changed area (km^2)				
		2006–2008	2008–2011	2011–2015	2015–2016	2016–2017
Primary forest	−569.40	−81.83	−38.15	−39.01	−88.38	−46.86
Secondary forest	−95.74	1.58	−31.86	−0.70	7.44	−7.96
Agropasture	306.04	81.58	61.44	−0.74	−40.97	2.49
Man-made bare land	91.73	0.31	1.46	32.66	−56.50	12.60
Natural bare land	213.35	42.17	−5.89	19.60	45.38	22.91
Water	54.01	−43.81	13.01	−11.81	133.02	16.82

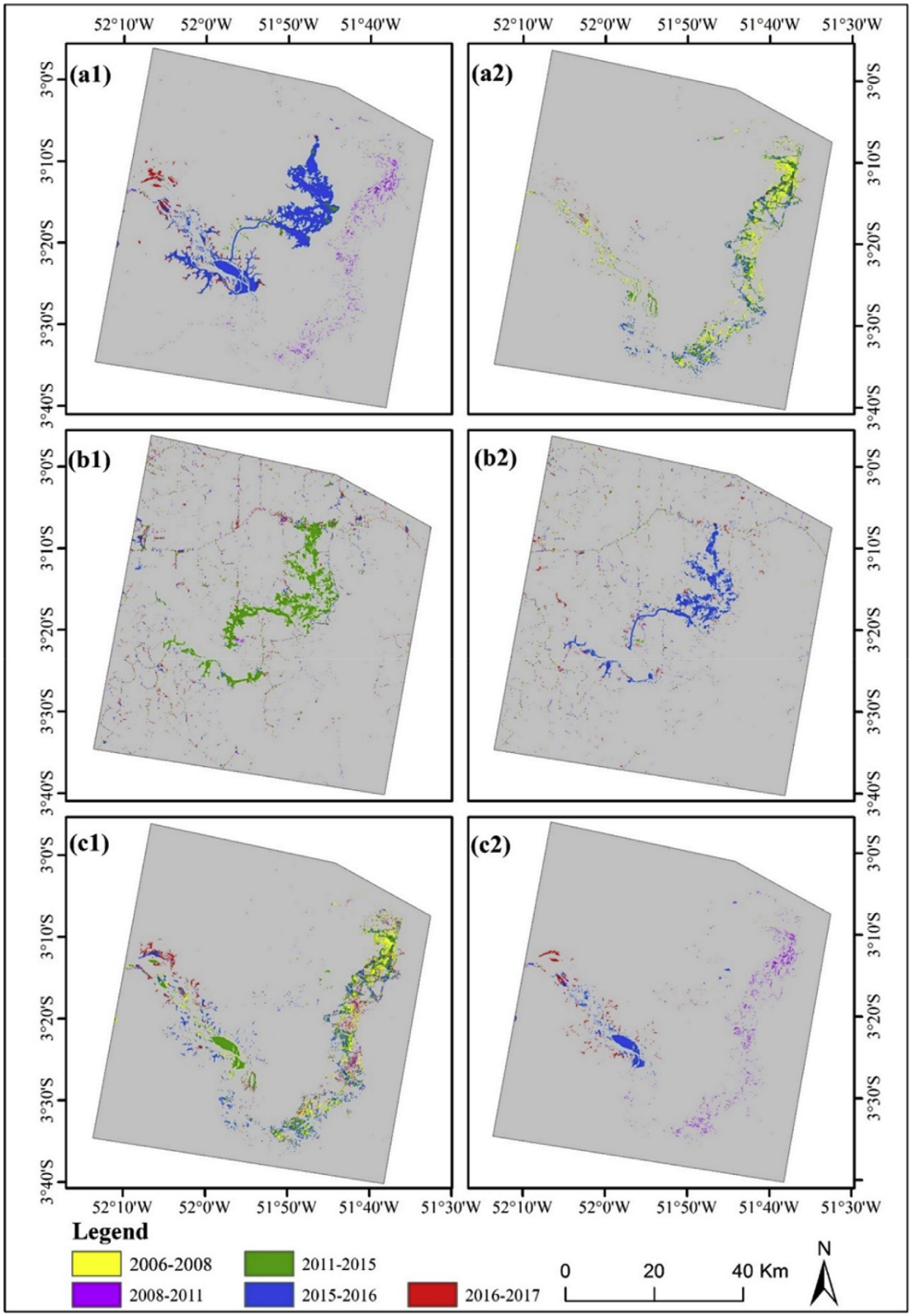

Fig. 4. Spatial distribution of land-cover change trajectories near the Belo Monte dam in Brazil during different detection periods. (a1), (b1), and (c1) represent the increased water, man-made bare land, and natural bare land, respectively; (a2), (b2), and (c2) represent the lost water, man-made bare land, and natural bare land, respectively.

along the canal (from the conversion of AP, ML, and NL to WA), and decreased downstream as it converted to NL. The changes in ML and NL were obvious due to the conversions between ML or NL and WA in different locations. Deforestation was obvious, but went to different land covers (e.g., SF, AP, NL, and WA). The change in AP was also obvious due to the AP expansion in some locations but AP conversion to ML or SF in other locations.

4) After completion stage (after 2016): The big change was the

Table 6
Annual changed area (km^2) of land-cover trajectories at different detection periods.

Major change	Change Trajectory	Annual changed area (km^2) at different detection periods				
		2006–2008	2008–2011	2011–2015	2015–2016	2016–2017
Water change	PF–WA	0.78	1.95	2.46	11.97	1.10
	SF–WA	0.08	0.20	0.64	15.07	2.06
	AP–WA	0.18	0.21	0.75	60.90	6.39
	ML–WA	0.00	0.02	0.03	72.06	5.70
	NL–WA	0.69	11.70	0.47	30.08	12.83
	Gain	1.74	14.07	4.35	190.08	28.06
	WA–ML	0.00	0.00	0.60	1.45	1.20
	WA–NL	42.49	0.74	13.96	54.65	9.71
	Loss	42.50	0.74	14.56	56.10	10.91
Man-made bare land change	PF–ML	0.41	0.25	12.12	6.18	4.01
	SF–ML	1.14	0.87	8.17	4.98	8.74
	AP–ML	4.26	4.19	15.91	27.32	27.85
	WA–ML	0.00	0.00	0.60	1.45	1.20
	Gain	5.82	5.31	36.81	39.93	41.80
	ML–SF	0.52	0.26	0.38	6.45	2.88
	ML–AP	4.97	3.50	3.79	18.53	21.61
	ML–WA	0.00	0.02	0.03	72.06	5.70
	Loss	5.49	3.77	4.20	97.04	30.19
Natural bare land change	PF–NL	0.85	4.81	5.17	10.65	13.00
	SF–NL	0.00	0.02	0.01	0.16	0.03
	AP–NL	0.17	0.24	0.46	6.19	9.45
	WA–NL	42.49	0.74	13.96	54.65	9.71
	Gain	43.51	5.81	19.60	71.64	32.19
	NL–WA	0.69	11.70	0.47	30.08	12.83
	Loss	0.69	11.70	0.47	30.08	12.83
Primary forest change	PF–SF	59.70	22.30	16.00	36.59	23.65
	PF–AP	25.08	14.86	16.84	39.20	25.58
	PF–ML	0.41	0.25	12.12	6.18	4.01
	PF–NL	0.85	4.81	5.17	10.65	13.00
	PF–WA	0.78	1.95	2.46	11.97	1.10
	Loss	86.83	44.17	52.60	104.59	67.33
Secondary forest change	PF–SF	59.70	22.30	16.00	36.59	23.65
	AP–SF	25.66	12.52	24.38	65.50	63.38
	ML–SF	0.52	0.26	0.38	6.45	2.88
	Gain	85.88	35.09	40.76	108.54	89.91
	SF–AP	83.30	64.28	30.44	73.43	79.14
	SF–ML	1.14	0.87	8.17	4.98	8.74
	SF–NL	0.06	0.16	0.65	5.51	4.79
	SF–WA	0.08	0.20	0.64	15.07	2.06
	Loss	84.59	65.51	39.91	98.98	94.73
Agropasture change	PF–AP	25.08	14.86	16.84	39.20	25.58
	SF–AP	83.30	64.28	30.44	73.43	79.14
	ML–AP	4.97	3.50	3.79	18.53	21.61
	Gain	113.35	82.64	51.07	131.16	126.33
	AP–SF	25.66	12.52	24.38	65.50	63.38
	AP–ML	4.26	4.19	15.91	27.32	27.85
	AP–NL	0.17	0.24	0.46	6.19	9.45
	AP–WA	0.18	0.21	0.75	60.90	6.39
	Loss	30.26	17.16	41.50	159.91	107.07

Note: PF, primary forest; SF, secondary forest; AP, agropoasture; ML, man-made bare land; NL, natural bare land; WA, water.

increased WA area upstream and the decreased WA area downstream. The increase upstream was due to filling the reservoir resulting in the conversion of different covers to WA, and the decrease of WA area downstream resulting in conversion to NL. The dynamic change between AP and ML, between SF and AP, and deforestation were also obvious.

5. Discussions

5.1. Improvement of land-cover classification and change detection results

Land-cover distribution is often mapped using classification algorithms such as traditional supervised classifier based on the spectral features of multispectral bands. However, spectral confusion is common for some land covers such as different forest types (e.g., advanced succession and primary forest) and non-vegetation types (e.g., bare soils and impervious surfaces). In this research, agricultural lands and pastures in the dry season, man-made bare soils in the construction areas, bare lands (bare soils, sands, mud) and shallow water along the river, and different impervious surfaces have similar spectral signatures, which could have resulted in misclassification. However, their different ecosystem functions make it possible to improve classification accuracy by modifying the classification results using expert rules. Since the post-classification comparison approach is based on the accurate classification of each image, it is critical to improve land-cover classification accuracy. Pixel-based classification approaches such as MLC, neural network, support vector machine, and decision tree classifier (G. Li et al., 2011, 2012; Lu et al., 2012) have been used extensively for land-cover classification, but proper use of object-based image classification can improve classification accuracy and reduce the common salt-and-pepper problem, especially when high spatial resolution images such as QuickBird are used (Lu, Hetrick, & Moran, 2010; Walsh et al., 2008).

Selection of suitable temporal resolution is an important part of

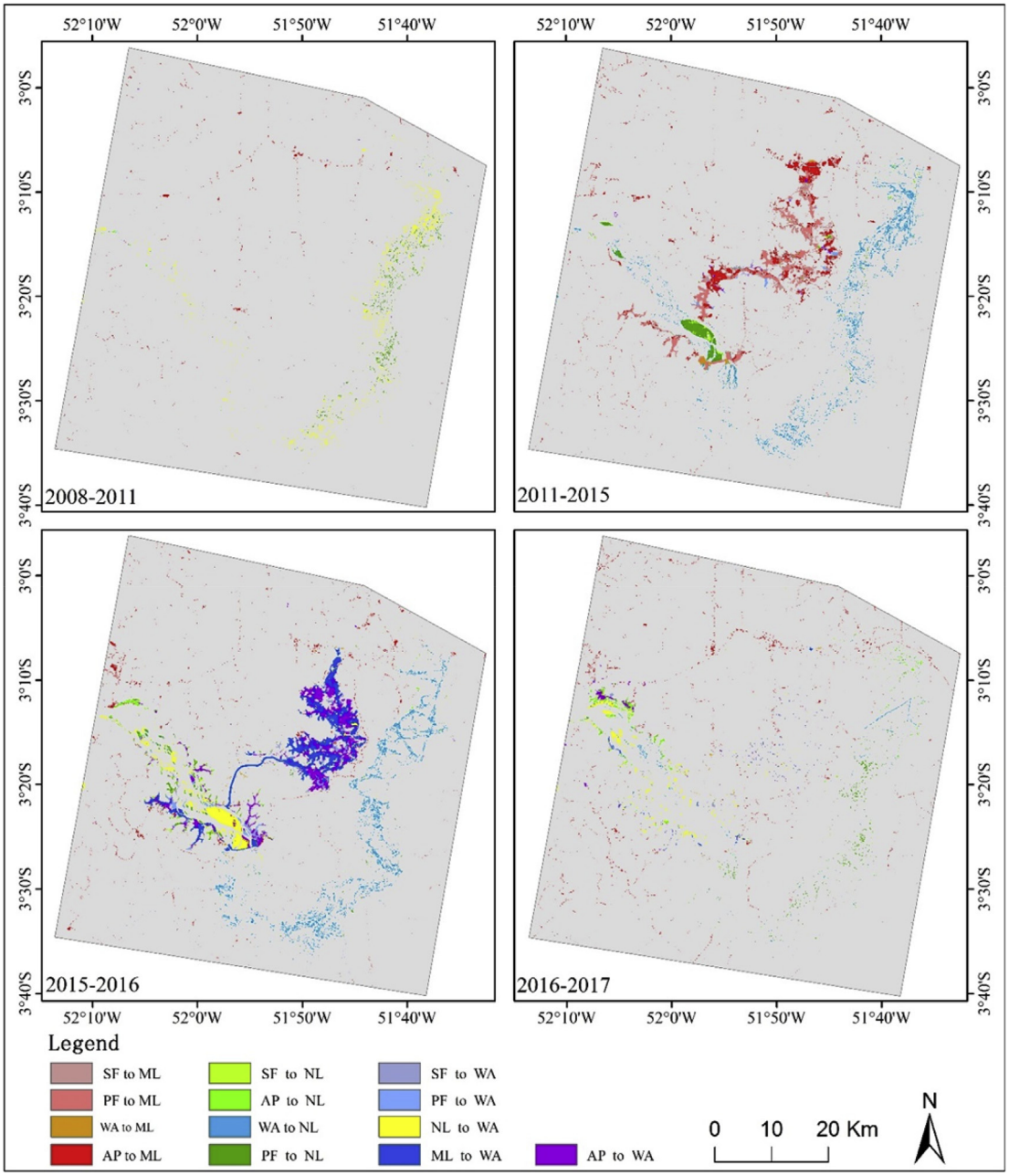

Fig. 5. Spatial distribution of major land-cover change trajectories upstream and downstream from Belo Monte dam site in Brazil during construction preparation (2008–2011), construction (2011–2015), and post-construction (2015–2016 and 2016–2017).

Table 7
Summary of upstream and downstream water areas (km^2).

Position	Total water areas (km^2) at different years					
	2006	2008	2011	2015	2016	2017
Upstream water	129.0	120.5	125.1	121.2	183.8	199.9
Downstream water	335.3	257.1	291.0	241.3	193.3	186.5
Total	464.3	377.6	416.1	362.5	377.1	386.4

land-cover change detection (Lu et al., 2014; Lunetta, Johnson, Lyon, & Crotwell, 2004; Reddy, Kumar, Kumar, & Shivapur, 2017; Sala, Parton, Joyce, & Lauenroth, 1988). Many factors affect this determination: the availability of remotely sensed data, the detection contents, the characteristics of the study area, and time and labor that can be required for the detection work. Land-cover change detection in the Brazilian Amazon basin is often difficult due to cloud cover (Asner, 2001). Our change detection results between 2011 and 2015 might not have captured the exact land-cover changes because cloud-free Landsat images were not available. In recent years, more sensor data such as Sentinel-2 and Landsat 8 OLI are available at no cost, and the application of Google Earth Engine technology provides a new platform for detecting detailed, short-term land-cover changes. Future research should focus on exploring the use of multisource data at short intervals for land-cover change detection.

5.2. The role and implication of dam construction on land-cover changes

Belo Monte has been a controversial project, with many opposed to its construction while others tout its benefits. There can be little doubt of the negative impacts such as blocking the fish migrations, the resettlement of over 25,000 people (FGV, 2015; Miranda Neto, 2014),

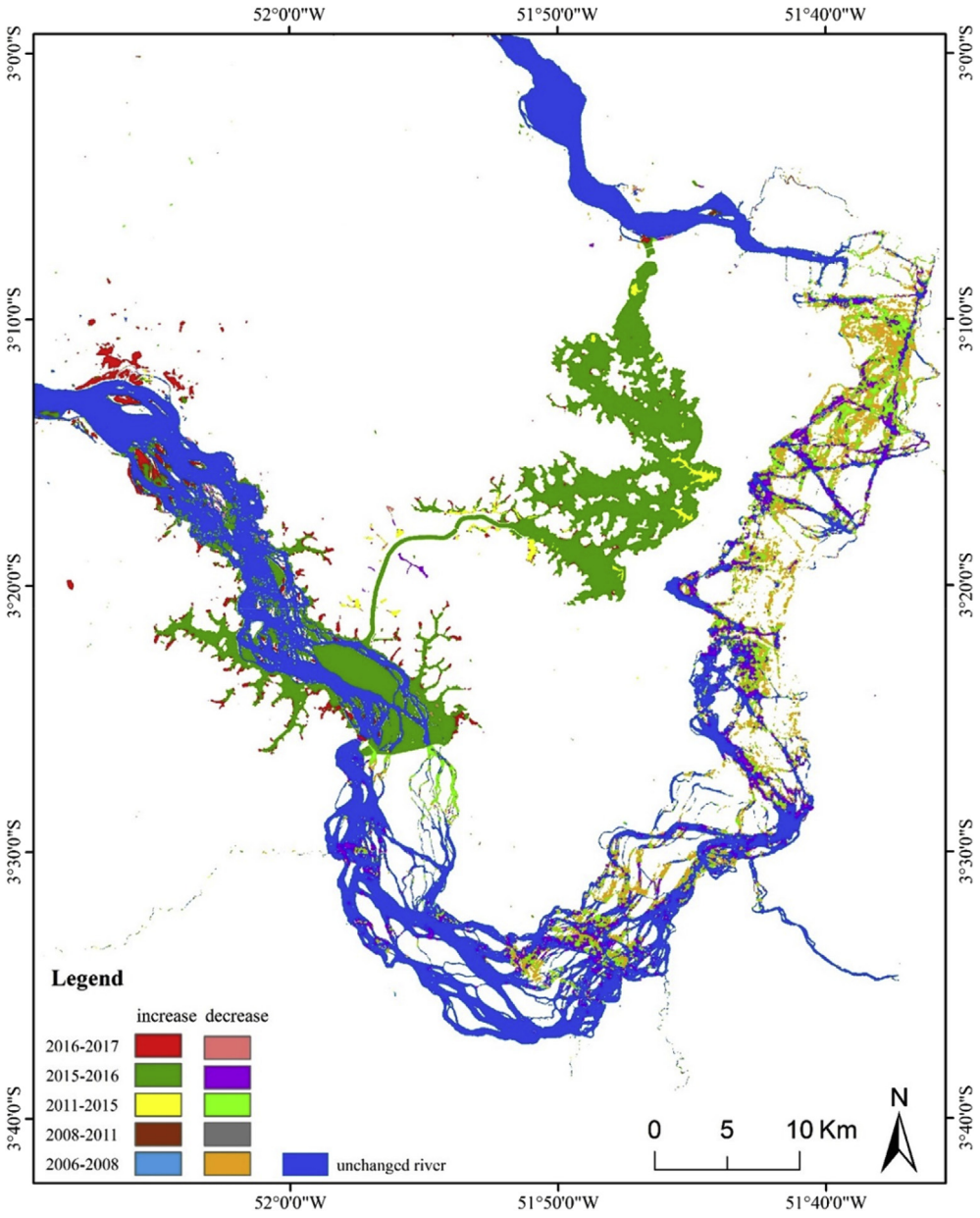

Fig. 6. Spatial distribution of water dynamic change in the area of the Belo Monte dam in Brazil at different detection periods.

and stressed social services for the urban population that doubled in a matter of two years during the peak of construction (Marin & Oliveira, 2016). Less discussed in the debate over the pros and cons of Belo Monte was the measurable changes in land cover that would result (Fearnside, 2017). This paper aims to correct this oversight. The land-cover change trajectories and change rates were related to the stages of dam construction. For example, before or at the initial stage of dam construction, deforestation and AP expansion were the major land-cover change processes observed in the landscape, and the changed areas were located away from the rivers and looked to the TransAmazon Highway, not to the river. The dam changed this focus. During the dam and canal construction stage, ML, including bare soils and impervious surfaces, sharply increased at the cost of forest and AP, with very large areas of farms, pastures, and forests changing to bare soil. By contrast, after the dam construction was completed, water area considerably increased upstream and decreased downstream. This relationship between land-cover changes and the dam construction stages provides a precise measure of the impact of the construction of the dam on the region's land cover. In the rush to produce hydropower, the construction companies, the government, and others interested in the project did not give adequate consideration to the land-cover changes they were causing, whom would be negatively affected by these changes, and whether adequate compensation would be provided. Recognition of these negative outcomes may have inspired the recent announcement by the Brazilian Ministry of Mines and Energy that they will no longer build megadams (Ventura, 2018). This was a surprising change in attitude by Brazil's government, which had long advocated building many more megadams. Whether this announcement represents a permanent change, or only a temporary respite, remains to be seen. Brazil already depends on hydropower for 67% of its energy generation (Aneel, 2017) and needs to consider diversification if it is to deal with climate change outcomes and reduce the negative impacts of megadams.

6. Conclusions

This research used Landsat time-series data to analyze land-cover changes and examined the impacts of the Belo Monte hydroelectric dam

Table 8
Summary of annual water and major land-cover changes in buffer zones.

Location	Change trajectories	Annual water changes (km^2) at different detection periods				
		2006–2008	2008–2011	2011–2015	2015–2016	2016–2017
Water change at upstream	PF–WA	0.10	0.33	0.53	5.98	0.50
	SF–WA	0.03	0.06	0.11	6.25	1.00
	AP–WA	0.03	0.04	0.11	14.76	3.96
	ML–WA	0.00	0.00	0.01	10.32	2.59
	NL–WA	0.10	1.43	0.19	26.67	11.58
	Gain	0.26	1.85	0.95	63.97	19.63
	WA–ML	0.00	0.00	0.20	0.16	0.07
	WA–NL	3.97	0.18	1.63	1.23	3.37
	Loss	3.97	0.18	1.83	1.39	3.44
Water change at downstream	PF–WA	0.62	1.54	1.12	3.12	0.04
	SF–WA	0.04	0.11	0.10	0.38	0.04
	AP–WA	0.09	0.08	0.05	0.34	0.04
	ML–WA	0.00	0.01	0.01	0.55	0.01
	NL–WA	0.58	10.21	0.26	1.82	0.00
	Gain	1.32	11.95	1.54	6.21	0.12
	WA–ML	0.00	0.00	0.30	0.45	0.43
	WA–NL	38.28	0.55	12.30	53.31	6.26
	Loss	38.28	0.55	12.60	53.77	6.69

Note: PF, primary forest; SF, secondary forest; AP, agropoasture; ML, man-made bare land; NL, natural bare land; WA, water.

construction on land-cover changes based on different construction stages. This research shows that without the impacts from dam construction, the major land-cover change in this region would have continued to be mainly deforestation and AP expansion. However, dam construction considerably increased these impacts on land-cover change amounts and trajectories. For example, before dam construction, deforestation (from PF to AP and SF), agricultural expansion (from PF and SF to AP), and the dynamic change between SF and AP dominated the land-cover change trajectories. During dam construction (2011–2015), although deforestation was still obvious, the conversion from PF to SF and the conversion from SF to AP were also common. Another important change was the increased area of ML near the dam and canal construction sites and the increased area of NL downstream. Near- or after-completion stages (2015–2017) witnessed the decreased area in PF, AP, and ML and large increased area in WA and NL, that is, considerably increased WA area upstream and along the canal and the decreased WA area downstream. Communities living downstream have already seen a big drop in the river water level, and their fishing activities are imperiled if not completely ruined for the foreseeable future. Upstream, many areas, including parts of the city of Altamira, were flooded and many vegetated areas had to be removed, or will die over the coming years as the permanent inundation damages their ability to survive. Resettled people who used to live by the river upstream from where the dam now sits are living in the city unable to use their fishing skills. Fishers despair of the lack of fish and their destroyed livelihoods. The consequences of these changes in land cover have a human face and consequences for human well-being that need to be addressed.

Note: The positive value indicates increased area, and negative value indicates decreased area from prior date to posterior date. The annual changed area was calculated: annual change area = [A(t2) – A(t1)]/(t2-t1), where A is the area of each land cover, and t1, and t2 are the detection periods at two dates.

Acknowledgments

This research was made possible by Michigan State University through research funds provided to Dengsheng Lu and Emilio F. Moran. FAPESP, through processo 2012/51465-0 awarded to Emilio Moran also provided support for this research paper. It has also been supported by NSF grant 1639115 to Moran as PI. Luciano Vieira Dutra and Miquéias Freitas Calvi thank CNPq for supporting fieldwork through grants #401528/2012-0, #309135/2015-0, and #409936 2013-8.

References

Aneel (2002). *Atlas de energia elétrica do Brasil.* Brasília: Aneel.
Aneel (2017). *Sistema de informações georreferenciadas do setor elétrico.* http://sigel.aneel.gov.br/sigel.html, Accessed date: 6 November 2017.
Asner, G. P. (2001). Cloud cover in landsat observation of the Brazilian Amazon. *International Journal of Remote Sensing, 22*, 3855–3862.
Bermann, C. (2001). *Energia no Brasil: Para que?, para quem? Crise e alternativas para uma país sustentável.* São Paulo: Editora Livraria da Física; FASE.
Brasil (2007). *Plano nacional de energia 2030.* Brasília: MME/EPE.
Chander, G., Markham, B. L., & Helder, D. L. (2009). Summary of current radiometric calibration coefficients for Landsat MSS, TM, ETM+, and EO-1 ALI sensors. *Remote Sensing of Environment, 113*, 893–903.
Chavez, P. S., Jr. (1996). Image-based atmospheric corrections: Revisited and improved. *Photogrammetric Engineering & Remote Sensing, 62*, 1025–1036.
Chen, G., Powers, R. P., de Carvalho, L. M. T., & Mora, B. (2015). Spatiotemporal patterns of tropical deforestation and forest degradation in response to the operation of the Tucurui hydroelectric dam in the Amazon basin. *Applied Geography, 63*, 1–8.
Congalton, R. G., & Green, K. (2008). *Assessing the accuracy of remotely sensed Data: Principles and practices* (2nd ed.). Boca Raton, FL: CRC Press.
Coppin, P., Jonckheere, I., Nackaerts, K., Muys, B., & Lambin, E. (2004). Digital change detection methods in ecosystem monitoring: A review. *International Journal of Remote Sensing, 25*, 1565–1596.
Erasu, D. (2017). Remote sensing-based urban land use/land cover change detection and monitoring. *Journal of Remote Sensing & GIS, 6*(2), 5.
Fearnside, P. M. (2003). Homem e ambiente na Amazônia. In P. M. Fearnside (Ed.). *A Floresta Amazônica nas mudanças globais* (pp. 1–18). Manaus: INPA.
Fearnside, P. M. (2014). Impacts of Brazil's Madeira River dams: Unlearned lessons for hydroelectric development in Amazonia. *Environmental Science & Policy, 38*, 164–172.
Fearnside, P. M. (2015). *Hidrelétricas na Amazônia: Impactos ambientais e sociais na tomada de decisões sobre grandes obras.* Manaus: Editora do INPA. http://fmclimaticas.org.br/wp-content/uploads/2015/07/Hidrel%C3%A9tricas-na-Amaz%C3%B4nia-Impactos-ambientais-Sociais..-V.1.pdf#page=37.
Fearnside, P. M. (2016). Environmental and social impacts of hydroelectric dams in Brazilian Amazonia: Implications for the aluminum industry. *World Development, 77*, 48–65.
Fearnside, P. M. (2017). *Belo Monte: Actors and arguments in the struggle over Brazil's most controversial Amazonian dam.* http://dx.doi.org/10.12854/erde-148-27 Die Erde.
Feng, Y., Lu, D., Moran, E. F., Dutra, L. V., Calvi, M. F., & Oliveira, M. A. F. (2017). Examining spatial distribution and dynamic change of urban land covers in the Brazilian Amazon using multitemporal multisensor high spatial resolution satellite imagery. *Remote Sensing, 9*(4), 381.
FGV (Fundação Getulio Vargas) (2015). *Mapa dos caminhos: Deslocamentos compulsórios no meio rural (Série Indicadores de Belo Monte).* http://indicadoresdebelomonte.eco.br/topics/3.
Foody, G. M. (2002). Status of land cover classification accuracy assessment. *Remote Sensing of Environment, 80*, 185–201.
Hage, J. A. A. (2012). A politica energética brasileira na era da globalização. *Revista de Sociologia E Política, 20*(41), 75–91.
Han, M., Zhang, C., & Zhou, Y. (2018). Object-wise joint-classification change detection for remote sensing images based on entropy query-by fuzzy ARTMAP. *GIScience and Remote Sensing.* http://dx.doi.org/10.1080/15481603.2018.1430100.
Karathanassi, V., Kolokousis, P., & Ioannidou, S. (2007). A comparison study on fusion methods using evaluation indicators. *International Journal of Remote Sensing, 28*, 2309–2341. http://dx.doi.org/10.1080/01431160600606890.

Laben, C. A.., and Brower B. V. 2000. reportProcess for enhancing the spatial resolution of multispectral imagery using Pan-Sharpening. Technical Report, US Patent No. 6011875. Rochester, NY: Eastman Kodak Company.

Li, G., Lu, D., Moran, E., & Hetrick, S. (2011). Land-cover classification in a moist tropical region of Brazil with Landsat Thematic Mapper imagery. *International Journal of Remote Sensing, 32*(23), 8207–8230. http://dx.doi.org/10.1080/01431161.2010.532831.

Li, G., Lu, D., Moran, E., & Sant'Anna, S. J. S. (2012). A comparative analysis of classification algorithms and multiple sensor data for land use/land cover classification in the Brazilian Amazon. *Journal of Applied Remote Sensing, 6*, 061706. http://dx.doi.org/10.1117/1.JRS.6.061706.

Li, M., Zang, S., Zhang, B., Li, S., & Wu, C. (2014). A review of remote sensing image classification techniques: The role of spatio-contextual information. *European Journal of Remote Sensing, 47*(1), 389–411. http://dx.doi.org/10.5721/EuJRS20144723.

Lu, D., Batistella, M., Li, G., Moran, E., Hetrick, S., Freitas, C., et al. (2012). Land use/cover classification in the Brazilian Amazon using satellite images. *Brazilian Journal of Agricultural Research, 47*(9), 1185–1208.

Lu, D., Hetrick, S., & Moran, E. (2010). Land cover classification in a complex urban-rural Landscape with QuickBird imagery. *Photogrammetric Engineering & Remote Sensing, 76*(10), 1159–1168 doi:0099-1112/10/7610–1159.

Lu, D., Li, G., & Moran, E. (2014). Current situation and needs of change detection techniques. *Internatinal Journal of Image Data Fusion, 5*, 13–38. http://dx.doi.org/10.1080/19479832.2013.868372.

Lu, D., Li, G., Moran, E., Dutra, L., & Batistella, M. (2011). A comparison of multisensor integration methods for land-cover classification in the Brazilian Amazon. *GIScience and Remote Sensing, 48*, 345–370. http://dx.doi.org/10.2747/1548-1603.48.3.345.

Lu, D., Li, G., Moran, E., & Hetrick, S. (2013). Spatiotemporal analysis of land-use and land-cover change in the Brazilian Amazon. *Internatinal Journal of Remote Sensing, 34*, 5953–5978.

Lu, D., Mausel, P., Brondízio, E., & Moran, E. (2004). Change detection techniques. *Internatinal Journal of Remote Sensing, 25*, 2365–2407.

Lunetta, R. S., Johnson, D. M., Lyon, J. G., & Crotwell, J. (2004). Impacts of imagery temporal frequency on land-cover change detection monitoring. *Remote Sensing of Environment, 89*(4), 444–454. http://dx.doi.org/10.1016/j.rse.2003.10.022.

Lu, D., & Weng, Q. (2007). A survey of image classification methods and techniques for improving classification performance. *International Journal of Remote Sensing, 28*, 823–870.

Maia, R. E. de F., Guerra, G. A. D., & Calvi, M. F. (2017). Dilemas do processo de desterritorialização de famílias atingidas por grandes projetos na Volta Grande do Xingu, Pará, Brasil. *Revista NERA, 20*(37), 195–215.

Marin, R. E. A., & Oliveira, A. C. (2016). Violence and public health in the Altamira region: The construction of the Belo Monte hydroelectric plant. *Regions and Cohesion, 6*(1), 116–134. http://dx.doi.org/10.3167/reco.2016.060106.

Mausel, P. W., Kramber, W. J., & Lee, J. K. (1990). Optimum band selection for supervised classification of multispectral data. *Photogrammetric Engineering & Remote Sensing, 56*, 55–60.

Miranda Neto, J. Q. (2014). Reassentamento da população urbana diretamente afetada pelo empreendimento hidrelétrico de Belo Monte em Altamira-PA. *Revista Nacional de Gerenciamento de Cidades, 2*(13), http://dx.doi.org/10.17271/231884722132014766.

Moran, E. F. (1975). The Brazilian colonization experience in the transamazon highway. *Anthropology, 16*(1), 29–57.

Moran, E. F. (1981). *Developing the Amazon.* Bloomington: Indiana University Press.

Moran, E. F. (2016). Roads and dams: Infrastructure-driven transformations in the Brazilian Amazon. *Ambiente & Sociedade, 19*(2), 207–220. http://dx.doi.org/10.1590/1809-4422ASOC256V1922016.

Moretto, E. M., Gomes, C. S., Roquetti, D. R., & Jordão, C. de O. (2012). Histórico, tendências e perspectivas no planejamento espacial de usinas hidrelétricas brasileiras: A antiga e atual fronteira Amazônica. *Ambiente & Sociedade, 15*(3), 141–164. http://dx.doi.org/10.1590/S1414-753X2012000300009.

Pohl, C., & van Genderen, J. L. (1998). Multisensor image fusion in remote sensing: Concepts, methods, and applications. *International Journal of Remote Sensing, 19*, 823–854.

Qiu, S., He, B., Zhu, Z., Liao, Z., & Quan, X. (2017). Improving Fmask cloud and cloud shadow detection in mountainous area for Landsats 4–8 images. *Remote Sensing of Environment, 199*, 107–119. http://dx.doi.org/10.1016/j.rse.2017.07.002.

Reddy, A., Kumar, M., Kumar, H. H., & Shivapur, A. V. (2017). Land use land cover change detection on Kanchinegalur sub watershed using GIS and remote sensing technique. *International Journal for Research in Applied Science and Engineering Technology, 5*(XI), 2128–2136.

Salah, M. (2017). A survey of modern classification techniques in remote sensing for improved image classification. *Journal of Geomatics, 11*(1), 21.

Sala, O. S., Parton, W. J., Joyce, L. A., & Lauenroth, W. K. (1988). Primary production of the central grassland region of the United States. *Ecology, 69*, 40–45.

Sevá, O. (2005). Povos indígenas, as cidades, e os beiradeiros do rio Xingu que a empresa de eletricidade insiste em barrar. In O. Sevá (Ed.). *Tenotã-Mõ. Alerta sobre as consequências dos projetos hidrelétricos no rio Xingu* (pp. 344). São Paulo: International Rivers Network.

Singh, A. (1989). Digital change detection techniques using remotely sensed data. *International Journal of Remote Sensing, 10*, 989–1003.

Tewkesbury, A. P., Comber, A. J., Tate, N. J., Lamb, A., & Fisher, P. F. (2015). A critical synthesis of remotely sensed optical image change detection techniques. *Remote Sensing of Environment, 160*, 1–14.

Ventura, M. (2018). Fase de grandes hidrelétricas chega ao fim. *O Globo*. https://oglobo.globo.com/economia/fase-de-grandes-hidreletricas-chega-ao-fim-22245669, Accessed date: 28 January 2018.

Vicente-Serrano, S. M., Perez-Cabello, F., & Lasanta, T. (2008). Assessment of radiometric correction techniques in analyzing vegetation variability and change using time series of Landsat images. *Remote Sensing of Environment, 112*, 3916–3934.

Walsh, S. J., McCleary, A. L., Mena, C. F., Shao, Y., Tuttle, J. P., González, A., et al. (2008). QuickBird and Hyperion data analysis of an invasive plant species in the Galapagos Islands of Ecuador: Implications for control and land use management. *Remote Sensing of Environment, 112*, 1927–1941.

Zhang, J. (2010). Multisource remote sensing data fusion: Status and trends. *International Journal of Image Data Fusion, 1*, 5–24.

Zhu, Z. (2017). Change detection using landsat time series: A review of frequencies, preprocessing, algorithms, and applications. *ISPRS Journal of Photogrammetry and Remote Sensing, 130*, 370–384. http://dx.doi.org/10.1016/J.ISPRSJPRS.2017.06.013.